J Mater Sci (2007) 42:2255–2260
DOI 10.1007/s10853-006-0649-8

Hydrogen permeation through internally oxidized Pd alloys

Viviane M. Azambuja · Dilson S. dos Santos

Received: 4 November 2005 / Accepted: 6 July 2006 / Published online: 30 January 2007

Abstract Hydrogen diffusivity and solubility were determined by electrochemical hydrogen permeation tests in samples of $Pd_{0.97}$ $Al_{0.03}$ and $Pd_{0.97}$ $Ce_{0.03}$ in the as received and internally oxidized conditions. Internal oxidization caused the appearance of nanosized oxide precipitates in the Pd matrix. The shape and size of precipitates and also the coherence between the precipitates and the matrix were observed by transmission electron microscopy (TEM). Electrochemical hydrogen permeation tests revealed that the presence of oxides increases the apparent hydrogen solubility, S_{app}, but decreases the hydrogen diffusivity, D_{app}. The values of D_{app} were 2.0×10^{-11} m^2 s^{-1} for vacuum heat treated $Pd_{0.97}$ $Al_{0.03}$ alloy and 4.0×10^{-12} m^2 s^{-1} for internally oxidized $Pd_{0.97}$ $Al_{0.03}$ alloy. However, the concentration of trapped hydrogen was 49 mol $H.m^{-3}$ for the $Pd_{0.97}$ $Al_{0.03}$ alloy in the vacuum heat treated condition and 403 mol $H.m^{-3}$ for the $Pd_{0.97}$ $Al_{0.03}$ alloy in the internally oxidized condition. Both heat treatments were performed at 1073 K for 24 h. The influence of the nature, size and distribution of the precipitates on the hydrogen permeation parameters are discussed in this paper.

Introdution

Palladium alloys, unlike many metals, have been attracting a great scientific interest due to their excellent physical properties with respect to hydrogen, especially their high solid solubility and high diffusivity. The insertion of a low concentration of oxidizable elements, such as Al, Zr, Ce, Cu and Cr, in the Pd matrix, can promote the oxidation of these elements and a composite alloy with ceramic nanoparticle dispersed in the Pd matrix can be created [1–3]. This occurs when these alloys are exposed to an oxidizing environment and high temperature for a sufficient amount of time to permit oxygen to diffuse through the metallic matrix. The requirements for this technique are that both the oxidizable element and the oxygen are soluble in the metal matrix and that the oxidizable element has a lower free energy of oxide formation than metal matrix itself [4].

The oxygen diffusivity coefficient in noble metals is the determining factor in achieving complete oxidation in these alloys. Other factors such as the time and the temperature of the heat treatment to promote internal oxidation, and crystallographic parameters of the oxide precipitates and matrix are important in the formation and final morphology of these oxide precipitates. The morphology of the oxide precipitates has a strong influence on the mechanical resistance of the alloy and can also increase the solid solubility and decrease the diffusivity of the hydrogen. This is due to the creation of new interfaces that trap the hydrogen in the alloy [5].

The main purpose of this work is to analyze the effect of internal oxidation on hydrogen diffusivity and solubility in the Pd alloys with Ce and Al by electrochemical permeation tests and TEM.

Experimental techniques

Buttons containing 5 g of the $Pd_{0.97}$ $Ce_{0.03}$ and $Pd_{0.97}$ $Al_{0.03}$ were melted by arc-melting in an argon atmo-

V. M. Azambuja (✉) · Dilson S. dos Santos
PEMM-COPPE, Universidade Federal do Rio de Janeiro,
P.O. Box 68505, 21941-972 Rio de Janeiro, RJ, Brazil
e-mail: vivianea@metalmat.ufrj.br

sphere, from pure elements (99.99% purity). Afterwards, samples were cold worked to a foil of about 100 μm in thickness. Next, the samples were heat treated at 1073 K for 24 h and 72 h in air to promote internal oxidation, and vacuum heat treated at 1073 K for 24 h. Then, the heat treatment samples were prepared metallographically and later submitted to electrochemical hydrogen permeation tests to analyze the hydrogen solubility and diffusivity. The ceramic nano-precipitate microstructure was investigated by TEM, using a Philips CM 300 microscope operating at 300 kV and equipped with an energy dispersive X-ray spectrometry for microanalysis (EDS), with a wavelength of 0.0196 Å. The samples were prepared for TEM analysis in a series of steps. First thin disks of 3 mm diameter were cut from the foils by ultrasonic drilling. Then the disks were carefully polished to a thickness of about 40 μm. Finally, the thinning and perforation of the samples were performed by argon ion milling using GATAN 600 model. The samples were thinned using two cannons at a 15° tilt, simultaneously bombarding the two faces of the sample. The milling time was 24–48 h depending on the sample thickness.

Samples with dimensions of 10×10 mm were submitted to electrochemical hydrogen permeation tests at ambient temperature using a solution of 0.1 N NaOH as electrolyte. These tests were undertaken using an electrochemical cell comprised of two compartments separated by the sample. In one of the compartments, a constant cathodic current was applied to generate hydrogen on the surface of the metal foil. In the other compartment, a weak anodic potential was applied to maintain a zero hydrogen concentration on the surface. Monitoring the anodic current, the diffusion rate of hydrogen through the sample (hydrogen flux) was recorded as a function of time until a steady state condition was achieved. For all samples the value of cathodic current density applied for hydrogen generation was 20 mA/m^2. The hydrogen generation side of the cell was subsequently kept under open circuit conditions and the specimen was allowed to outgas. The evolution of the hydrogen flux, J_L with time (t), exhibits a sigmoidal relationship. Assuming the diffusivity of hydrogen is not varying with the increase in concentration, this flux may be expressed as [6]:

$$J_L(t) = J_\infty \left(1 - \frac{4}{\pi} \sum_0^\infty \frac{(-1)^n}{2n+1} \exp\left(\frac{(-(2n+1)^2 \pi^2 D_{\text{app}}(t)}{4L^2}\right)\right) \quad (1)$$

where J_∞ is the steady state flux, D_{app} is the apparent hydrogen diffusivity, L is the sample thickness and n is the term of series which is $n = 1,2,3 \ldots$.

The hydrogen diffusivity can be determined by curve fitting using Eq (1). In cases where the curves indicate deep traps, it is better to calculate the hydrogen diffusivity by the intersection of the tangent at the inflection point of the hydrogen permeation curve with the initial level $J_L(t) = 0$ to yield the break through time, t_b [6]

$$t_b = \frac{0,76L^2}{\pi^2 D_{\text{app}}} \quad (2)$$

In the steady regime, the hydrogen solubility can be determined by applying the following equation:

$$S_{\text{app}} = \frac{1}{L} \int_0^t J_L(t) \mathrm{d}t \quad (3)$$

Results and discussion

After an oxidizing treatment, one at 1073 K for 24 h and the other at 1073 K for 72 h, for the $Pd_{0.97}$ $Al_{0.03}$ and $Pd_{0.97}$ $Ce_{0.03}$ alloys, nano-precipitates of Al_2O_3 and CeO_2 were observed in the Pd matrix, as shown in Fig. 1. The precipitates were characterised by both EDS microanalyses in the TEM and selected area electron diffraction (SAED). In the Al-containing alloy, which was heat treated at 1073 K for 24 h and 72 h, prismatic α-Al_2O_3 nano-precipitates of around 20 nm in size were observed dispersed in the Pd matrix. However, in the $Pd_{0.97}$ $Al_{0.03}$ alloy, which was heat treated at 1073 K for 72 h, larger round precipitates of around 50 nm were also observed. In the Ce-containing alloy, the fine acicular CeO_2 precipitates were observed as rod-like particles 2–3 μm in length and with a circular cross-section morphology around 20–40 nm in diameter. These CeO_2 precipitates exhibited preferential growth directions within the Pd matrix, emphasizing that the Al and Ce precipitates have a completely different shape and size.

High Resolution Transmission Electron Microscopy (HRTEM) studies have provided important information on the atomic structure of metal/oxide interfaces and, for limited cases, on interfacial chemistry resulting from internal oxidation [3, 4]. Such metal/oxide interfaces have been investigated for a variety of oxide structures, for example cubic oxides

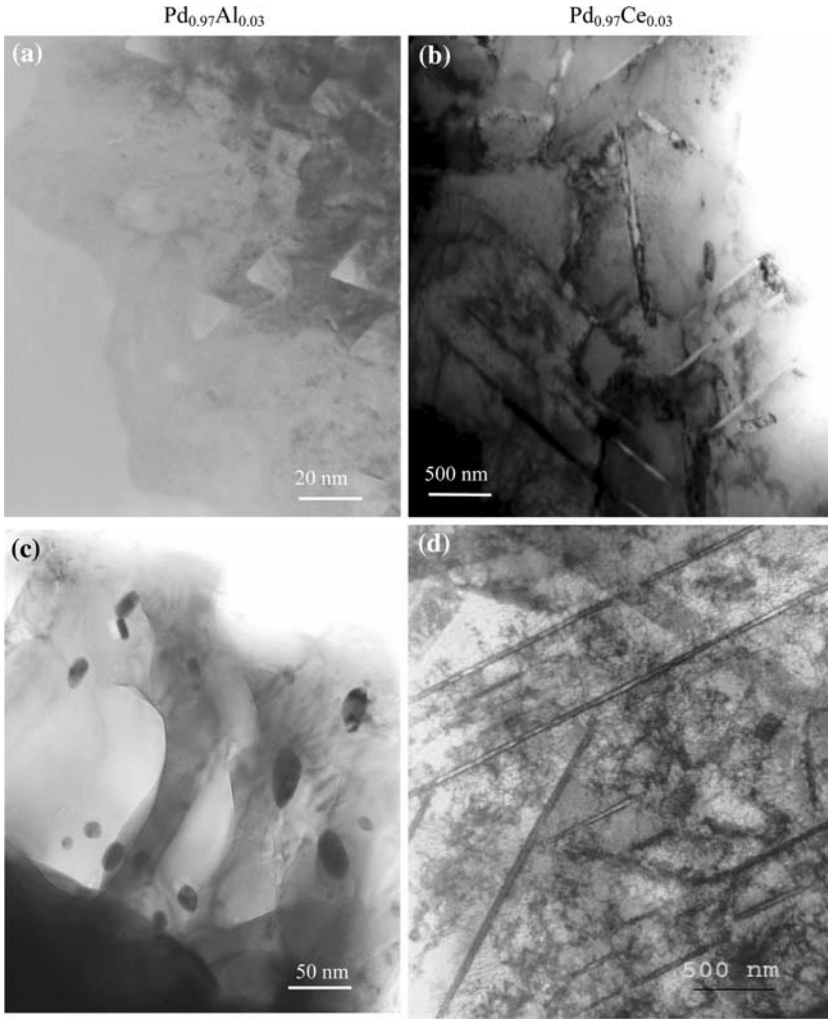

Fig. 1 TEM micrographs for $Pd_{0.97}$ $Al_{0.03}$ heat treated at 1073 K for 24 (**a**) and 72 h (**c**) and $Pd_{0.97}$ $Ce_{0.03}$ alloys heat treated at 1073 K for 24 (**b**) and 72 h (**d**)

Ag/CdO [1], Cu/MgO, Pd/MgO [4], Cu/η-Al_2O_3 and Pd/η-Al_2O_3 [7], tetragonal oxides Pd/TiO_2 and Cu/TiO_2 [4], hexagonal oxide Pd/ZnO [1] or trigonal oxide Pd/α-Al_2O_3 [4]. In the metal-Al-O_2 system, numerous metastable crystal structures of alumina are formed by internal oxidation including cubic γ and η, tetragonal δ, and monoclinic θ phases, in addition to the stable trigonal α-Al_2O_3 phase [4, 7, 8]. Interfacial studies on the stable α-Al_2O_3 phase are more important from a technological point of view, because this structural form is used extensively, for instance as fiber reinforcement in composite materials or as substrate in electronic packaging.

There are many factors which can influence the morphology of the oxide precipitate formed in a matrix during the internal oxidation heat treatment. These include the time and temperature of the heat treatment, the difference between the nucleation and the growth rate of the precipitate, the oxygen diffusivity in the alloys, the crystallographic structure of the oxide, and the orientation relationship (crystal symmetry) between the oxide and the Pd matrix [9, 10].

The presence of the CeO_2 and Al_2O_3 oxides formed during internal oxidation of the alloys studied, decreased the hydrogen diffusivity but considerably increased the hydrogen solubility as compared to the respective samples before heat treatment. The amount of hydrogen trapped by the ceramic/matrix interface and the hydrogen diffusivity were calculated from hydrogen permeation curves obtained by electrochemical hydrogen permeation testing.

Figure 2 shows the hydrogen permeation behavior for $Pd_{0.97}$ $Al_{0.03}$ in the vacuum heat treated condition, in which hydrogen sorption and desorption curves, obtained after the steady stage condition was achieved, are presented. Taking into account the displacement of the experimental desorption curve from the equation $(1–J_L(t)/J_\infty)$, it is possible to calculate the area between the two curves which represents the amount of hydrogen trapped in the material (49 molH.m^{-3}).

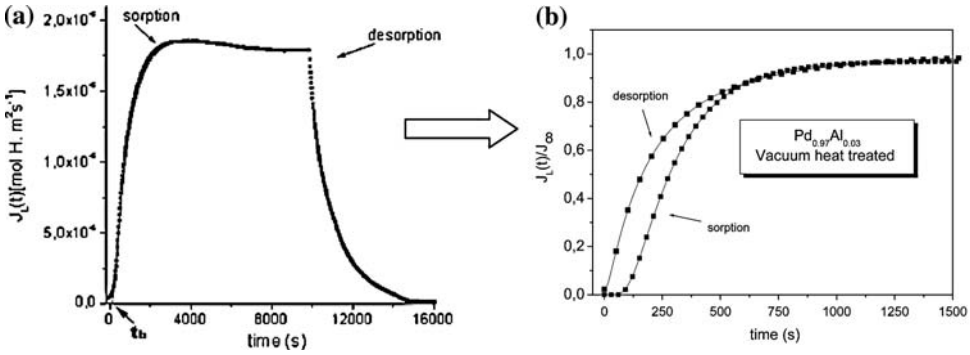

Fig. 2 Hydrogen permeation curves (sorption/desorption) for $Pd_{0.97}$ $Al_{0.03}$ alloy vacuum heat treated and (**b**) the area between the two curves represents the amount of hydrogen trapped in the material

Figure 3 shows the hydrogen permeation curves (sorption/desorption) for the $Pd_{0.97}$ $Ce_{0.03}$ and $Pd_{0.97}$ $Al_{0.03}$ alloys respectively, which permit the calculation of the hydrogen diffusivity and solubility. Hydrogen solubility refers to the hydrogen dissolved in the octahedral sites, at grain boundaries and at dislocations. A low dislocation density was observed, due to the heat treatment and the Al in solid solution within Pd matrix. The resulting hydrogen diffusivity and solubility determinations allow a comparison between the effects of the hydrogen interaction with the specific microstructure corresponding to each heat treatment condition. In these cases, the area between the two curves represents the level of hydrogen trapped by the defects (oxide). For the $Pd_{0.97}$ $Al_{0.03}$ alloys, the 72 h heat treated material exhibited a higher level of hydrogen trapping than the 24 h material. This is due to the large amount of alumina precipitates within the Pd matrix in this alloy. The same behaviour is observed for the $Pd_{0.97}Ce_{0.03}$ alloys. The heat treatment at 1073 K for 24 h was not sufficient to promote complete oxidation ($\approx$ 120 μm in thickness) of the oxidizing elements dissolved in the Pd matrix as reported by Noh et al [2]. The internal oxidation involves the nucleation and growth of the oxides in the Pd matrix. It is expected that for a short period of time (24 h), nucleation is privileged. For longer periods of time at the same temperature, it is expected that not only the formation of nuclei but also the growth of these precipitates will occur. For this reason an increase in the hydrogen trapping in the alloy is observed with for increased heat treatment times [9].

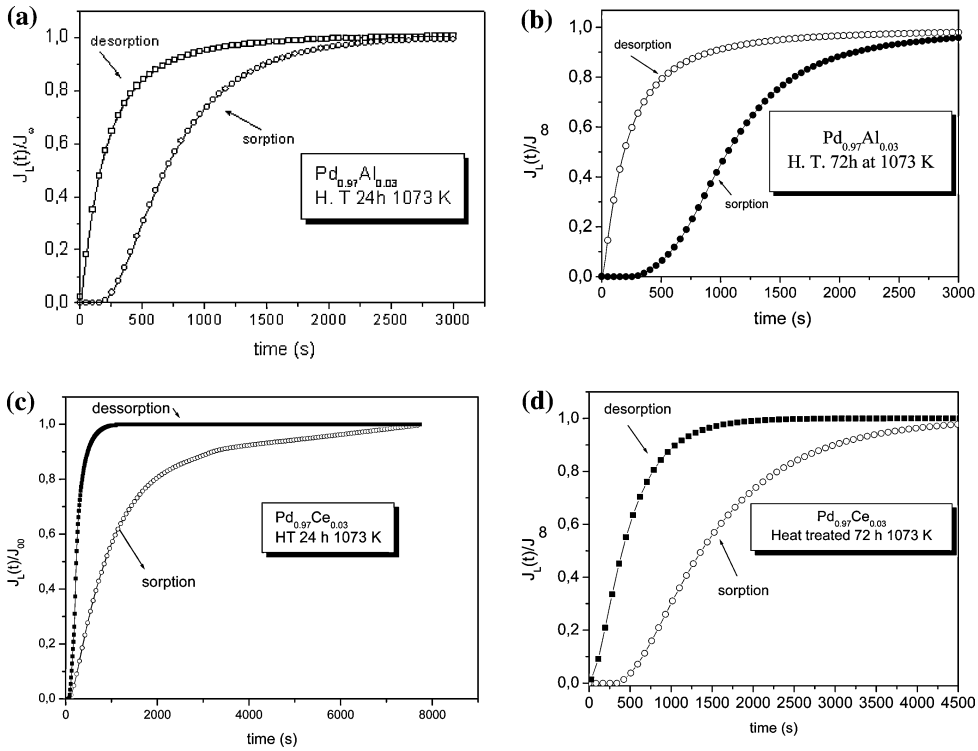

Fig. 3 Hydrogen permeation curves (sorption/desorption) for $Pd_{0.97}$ $Ce_{0.03}$ and $Pd_{0.97}$ $Al_{0.03}$ alloys heat treated at 1073 K for 24 and 72 h

The hydrogen permeation curves for both the $Pd_{0.97}$ $Ce_{0.03}$ and $Pd_{0.97}$ $Al_{0.03}$ alloys presented in Fig. 3 indicate a high level of hydrogen trapped in the microstructure due to the presence of oxide precipitates. These oxide precipitates result in irreversible trapping [1] and are also effective in increasing the total number of hydrogen traps in the material. They also cause stress concentrations in regions in the Pd matrix that induce a further increase in hydrogen trapping, especially when the precipitates are coherent with the matrix.

The Al_2O_3 precipitates are nanometric in size and coherent with the Pd matrix. They cause high tensile stresses in the Pd matrix, evidence of which can be observed by the brittle aspect of the $Pd_{0.97}$ $Al_{0.03}$ alloy. This brittleness can be explained by the high precipitate density and the high tensile stresses caused by the structural differences due to the relative lattice parameters and the volume of the Pd matrix (58.86 $Å^3$) and Al_2O_3 precipitates (254.25 $Å^3$). The $Pd_{0.97}$ $Ce_{0.03}$ alloys did not exhibit the brittleness which the $Pd_{0.97}$ $Al_{0.03}$ alloys had. The internal oxidation promoted hardening in the palladium due to the formation of a high density of these long precipitates in the matrix. The distortion created by these precipitates caused strengthening of the $Pd_{0.97}$ $Ce_{0.03}$ alloy. This suggests that the presence of cerium oxide precipitates, due to their crystallographic nature, promote an accommodation of the localized tension at the precipitate/matrix interface.

Table 1 shows the hydrogen diffusivity and the amount of trapped hydrogen for the $Pd_{0.97}$ $Al_{0.03}$ and $Pd_{0.97}$ $Ce_{0.03}$ alloys heat treated for different times. It is observed that, for the $Pd_{0.97}$ $Al_{0.03}$ alloys, the hydrogen diffusivity decreases and the amount of trapped hydrogen increases most for the sample that is heat treated for the longest time. The same was observed for the $Pd_{0.97}$ $Ce_{0.03}$ alloys. The CeO_2 precipitates trap more hydrogen than the Al_2O_3. The different shapes and sizes of the oxide precipitates, which were formed within Pd matrix of the alloys, exert a strong influence on hydrogen trapping. The determining factors for the increase in hydrogen solid solubility, which is due to the precipitation, are the nature of the interface (coherent or incoherent), the volumetric fraction and the electronic structure. Both precipitates (Al_2O_3 and CeO_2) exhibit coherent interfaces with the Pd matrix; therefore, they have a better ability to trap hydrogen. Furthermore, the misfit structural of the precipitates with respect to the crystalline matrix, which contributes to the increase of material hardness should also be taken into account [10].

Figure 4 shows both the hydrogen solubility variation for the different heat treatments to which the $Pd_{0.97}$ $Al_{0.03}$ alloy was submitted [11] and a schematic model of the respective microstructures. It also compares the hydrogen solubility of pure palladium and the $Pd_{0.97}$ $Al_{0.03}$ alloy. The hydrogen solubility changes according to the different structures which are result from the different heat treatments applied. In the $Pd_{0.97}$ $Al_{0.03}$ alloy in the vacuum heat treated condition, there is only Al in solid solution. In the $Pd_{0.97}$ $Al_{0.03}$ alloy in the cold worked condition, there is Al in solid solution and also a high dislocation density resulting from the plastic strain. In the $Pd_{0.97}$ $Al_{0.03}$ alloy heat treated for 24 h, there are small Al_2O_3 precipitates dispersed in Pd matrix, and finally in the $Pd_{0.97}$ $Al_{0.03}$ alloy heat treated for 72 h, there are Al_2O_3 precipitates which are larger and more widely-spaced than in the

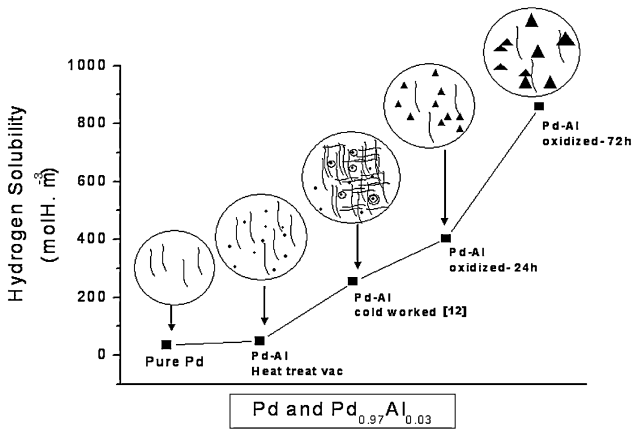

Fig. 4 The hydrogen solubility variation for pure Pd and $Pd_{0.97}$ $Al_{0.03}$ alloys with different heat treatments and a schematic model of the respective microstructures. Obtained from hydrogen permeation curves at 298 K and under 1 atm condition

Table 1 Hydrogen diffusivity and trapped in pure Pd, $Pd_{0.97}$ $Al_{0.03}$ and $Pd_{0.97}$ $Ce_{0.03}$ alloys at 298 K and under 1 atm condition

Samples	D_{app} (m^2 s^{-1})	Hydrogen trapped	
		(mol $H.m^{-3}$)	[H/Pd]
Pure Pd VHT	$5{,}5 \times 10^{-11}$	22	$[2 \times 10^{-3}]$
$Pd_{0.97}$ $Al_{0.03}$ VHT	2.0×10^{-11}	49	$[4.4 \times 10^{-3}]$
$Pd_{0.97}$ $Al_{0.03}$ HT24 h	4.0×10^{-12}	403	$[36 \times 10^{-3}]$
$Pd_{0.97}$ $Al_{0.03}$ HT72 h	2.3×10^{-12}	859	$[76 \times 10^{-3}]$
$Pd_{0.97}$ $Ce_{0.03}$ HT 24 h	6.3×10^{-12}	1064	$[166 \times 10^{-3}]$
$Pd_{0.97}$ $Ce_{0.03}$ HT 72 h	1.1×10^{-12}	1178	$[105 \times 10^{-3}]$

$Pd_{0.97}$ $Al_{0.03}$ alloy heat treated for 24 h. In the vacuum heat treated $Pd_{0.97}$ $Al_{0.03}$ alloy, the hydrogen solubility is slightly higher than in the pure Pd. This is due to the distortions due to the presence of Al atoms in the Pd matrix. Such regions of high local distortion acting as hydrogen traps. In the $Pd_{0.97}$ $Al_{0.03}$ alloy, which was heat treated the longest, the hydrogen solubility is higher than the $Pd_{0.97}$ $Al_{0.03}$ alloy with the shortest heat treatment. This is due to larger size of the alumina precipitates which have a stronger influence on hydrogen solubility. Although the smaller precipitates, coherent with the matrix are more effective in hydrogen trapping than is the case for the semi-coherent or incoherent precipitates, the duration of the internal oxidation heat treatment applied to the $Pd_{0.97}$ $Al_{0.03}$ alloy treated for 24 h was not enough to obtain complete oxidation. Whereas, the $Pd_{0.97}$ $Al_{0.03}$ alloy heat treated for 72 h did achieve complete oxidation, exhibiting a higher density of precipitates, which, in turn, represents more interfaces to trap the hydrogen.

The increase in hydrogen solubility between palladium and vacuum heat treated $Pd_{0.97}$ $Al_{0.03}$ alloys is much smaller than that between palladium and internally oxidized $Pd_{0.97}$ $Al_{0.03}$ alloy.

Conclusion

The oxidation heat treatment at 1073 K for 24 and 72 h on $Pd_{0.97}$ $Al_{0.03}$ and $Pd_{0.97}$ $Ce_{0.03}$ promotes the formation of prismatic Al_2O_3 nano-precipitates and needle-shaped CeO_2, respectively. The $Pd_{0.97}$ $Al_{0.03}$ alloy, heat treated at 1073 K for 72 h, induces more nucleation of Al_2O_3 precipitates dispersed in Pd matrix than the same alloy heat treated for 24 h. However, the $Pd_{0.97}$ $Ce_{0.03}$ alloy, heat treated at 1073 K for 72 h, induces only the growth of the CeO_2 precipitates. Both of these precipitates decrease the hydrogen diffusivity and increase the hydrogen solubility when compared with the same alloys without oxide precipitates. It is possible to calculate the amount of hydrogen trapped in the material from the area between the hydrogen sorption and desorption curves. The hydrogen solubility increases with the increase of heat treatment time for the both $Pd_{0.97}$ $Al_{0.03}$ and $Pd_{0.97}$ $Ce_{0.03}$ alloys. The CeO_2 precipitates trap more hydrogen than the Al_2O_3 ones.

Acknowledgements The authors acknowledge CAPES, CNPq and Faperj.

References

1. Huang X, Mader W, Kirchheim R (1991) Acta Metallurgica Materialia 39:893
2. Noh H, Flanagan TB, Balasubramaniam R, Eastman JA (1996) Scripta Materialia 34(6):863
3. J. Meijering (1971) In H. Hermann (ed) Advances in Materials Reserch. Wiley, New York, pp.1–81
4. Cosandey F, Lu P (1994) Acta Metallurgica Materialia 42(6):1913
5. Azambuja VM, Dos Santos DS, Pontonnier L, Miraglia S, Fruchart D (2002) Journal of Alloys and Compounds 346 (1–2):142
6. N. Boes, H. Zuchner, Less J (1976) Common Metals 49:223
7. Muschik T, Rühle M (1992) Philosophical Magazine A65:363
8. Eastman JE, Rühle M (1989) Ceramics Engineering Science Proceedings 10:1515
9. Kooi BJ, Hosson De JThM (2000) Acta Materialia 48:3687–3699
10. Azambuja VM, Dos Santos DS, Pontonnier L, Morales M, Fruchart D (2006) Scripta Materialia 54:1779–1783
11. dos Santos DS, Azambuja VM, Pontonnier L, Miraglia S, Fruchart D (2003) Journal of Alloys and Compounds 356–357:236–239